REPORT DOCUMENTATION PAGE

Form Approved
OMB No 0704-0188

1. AGENCY USE ONLY (LEAVE BLANK)	2. REPORT DATE	3. REPORT TYPE AND DATES COVERED
	December 1996	Technical Paper

4. TITLE AND SUBTITLE

Studies of Artificial Cracks at Rocket Motor Liners by the Frozen Stress Method

5. FUNDING NUMBERS

C: Sub: 95-7025-K-1169
PE: 62601F
PR: 2302
TA: M1G2

6. AUTHOR(S)

C.W. Smith and E.F. Finlayson, VPI
C.T.Liu, OL-AC PL/RKS

7. PERFORMING ORGANIZATION NAME(S) AND ADDRESS(ES)

Department of Engineering Science and Mechanics
Virginia Polytechnic Institute and State University
Blacksburg VA 24061

8. PERFORMING ORGANIZATION REPORT NUMBER

9. SPONSORING/MONITORING AGENCY NAME(S) AND ADDRESS(ES)

Phillips Laboratory (AFMC)
OL-AC PL/RK3
10 East Saturn Blvd.
Edwards AFB CA 93524-7680

10. SPONSORING/MONITORING AGENCY REPORT NUMBER

PL-TP-97-3038

11. SUPPLEMENTARY NOTES

COSATI CODE(S): 210902

Available from CPIA. Published in 1996 JANNAF Structures and Mechanical Behavior Subcommittee Meeting, CPIA Publication 652, Dec 96, pp. 201-211

12a. DISTRIBUTION/AVAILABILITY STATEMENT

Approved for Public Release; Distribution is unlimited

12b. DISTRIBUTION CODE

A

13. ABSTRACT (MAXIMUM 200 WORDS)

A preliminary investigation limited to stress freezing materials was undertaken in order to develop a test method for estimating the stress intensity factor (SIF) distribution along the border of cracks in the bond line of a bi-material specimen. It was desired to measure the influence of residual stress and mixed mode effects for such specimens. A single edge notched specimen was selected, and a test procedure was devised for isolating the residual stress effect at the bond line for Mode I. Subsequently, mixed mode tests were conducted in the absence of externally induced residual stress and the SIF distribution for K_1 and K_2 were obtained. It was found that the level of the SIF values were increased by the bond line in cracked homogeneous bondline specimens for bondlines nearly normal to the applied load but that this effect was not increased in bonded bimaterial specimens. For larger angles of inclination to a normal to the applied load no increase in the SIF above the homogeneous result was found.

14. SUBJECT TERMS

bondline specimens; stress intensity factor; cracks

15. NUMBER OF PAGES

11

16. PRICE CODE

17. SECURITY CLASSIFICATION OF REPORT	18. SECURITY CLASSIFICATION OF THIS PAGE	19. SECURITY CLASSIFICATION OF ABSTRACT	20. LIMITATION OF ABSTRACT
Unclassified	Unclassified	Unclassified	SAR

STUDIES OF ARTIFICIAL CRACKS AT ROCKET MOTOR LINERS BY THE FROZEN STRESS METHOD

C. W. Smith and E.F. Finlayson
Department of Engineering Science and Mechanics
Virginia Polytechnic Institute and State University
Blacksburg, VA 24061

C. T.Liu
OL-AC PL/RKS
Phillips Laboratory
10 E. Saturn Blvd.
Edwards AFB, CA 93524-7680

ABSTRACT

A preliminary investigation limited to stress freezing materials was undertaken in order to develop a test method for estimating the stress intensity factor (SIF) distribution along the border of cracks in the bond line of a bi-material specimen. It was desired to measure the influence of residual stress and mixed mode effects for such specimens. A single edge notched specimen was selected, and a test procedure was devised for isolating the residual stress effect at the bond line for Mode I. Subsequently, mixed mode tests were conducted in the absence of externally induced residual stress and the SIF distributions for K_1 and K_2 were obtained. It was found that the level of the SIF values were increased by the bond line in cracked homogeneous bondline specimens for bondlines nearly normal to the applied load but that this effect was not increased in bonded bimaterial specimens. For larger angles of inclination to a normal to the applied load no increase in the SIF above the homogeneous result was found.

INTRODUCTION

When a crack is located at the interface between two materials, near tip stress analysis is complicated by the fact that the mode 1 and mode 2 stress intensity factors (SIF) cannot be decoupled [1]. However, if the materials are incompressible, and plane strain exists, the near tip interface equations reduce to the more familiar form for isotropic and homogeneous elastic solids [2].

When cracks occur between a solid rocket motor and its rubber liner, the above conditions are approximately realized and occur at a rather low modulus ratio between the two materials. The first author and his colleagues have had considerable success in measuring three dimensional effects in cracked isotropic and homogeneous bodies using a refined frozen stress method [3]. The frozen stress method is briefly summarized in Appendix I. In order to explore the feasibility of such an approach in measuring three dimensional and residual stress effects in such cracks as described above, a series of experiments were conducted on thick plates in tension containing bondline cracks between two different incompressible materials.

The experiments can be divided into two parts:

i. A study of externally induced residual stress effects on a bond line crack under Mode I loadings and
ii. A study of mixed mode effects in the absence of externally induced residual stresses.

SPECIMEN CONFIGURATION, MATERIALS AND TEST PROGRAM

The specimen configuration used in all tests is pictured in Fig. 1. All loads were parallel to the long dimension of the specimens. The materials and their properties are given in Table I.

Table I

Material	T_{critical}	E_{Hot}	f_r
Araldite	240°F	2698 psi (18.60 MPa)	1.64 psi-in (286.9 Pa-m)
Aral-Alum	240°F	5349 psi (36.88 MPa)	____

The thermal coefficient of expansion for both materials was matched exactly at 15.3 x 10^{-6} per $°F$ at room temperature and 119 x $10^{-6} \pm 20$ x10^{-6} per $°F$ at 240°F. The, Araldite-aluminum specimens were produced in opaque form by adding 25% by weight of aluminum powder to the pure transparent araldite, a common photoelastic material. The bonding agent was a commercial glue PLM-9 made by Photoelastic, Inc. Raleigh, NC. The test specimen materials were supplied by Survey Technology Centre, London.

The testing program involved three test specimens for each crack orientation: one homogeneous specimen (B-1), one bonded homogeneous specimen (B-2) and one bonded bimaterial specimen (B). This was done in order to isolate residual bond line effects from bimaterial effects.

ANALYTICAL PROCEDURES

In order to provide an analytical control, the following procedure was used to estimate theoretical values of $K_{1(th)}$ and and $K_{2(th)}$.

The values of $K_{1(th)}$ and $K_{2(th)}$ were based on two dimensional solutions for edge cracks in semi-infinite plates [4], [5] adjusted to finite width plates using [6], [7] and correcting for the notch effect using [8]. In adjusting the infinite plate solution to the finite plate solution for inclined cracks ($\beta \neq 0$), the projection of the crack normal to the direction of the applied load was used.

Experimental results were obtained from frozen stress photoelastic experiments and optical data were converted into stress intensity values using the algorithms and procedures described in Appendix II.

TEST RESULTS

RESIDUAL STRESS TESTS

In order to generate a residual stress field, three specimens B-1, B-2 and B with $\beta = 0$ (Fig. 1) were cycled to 280°F to exacerbate the thermal coefficient variations at elevated temperature between the araldite and the araldite-aluminum materials. Then after stress freezing using the 280°F maximum temperature, thin slices were removed mutually orthogonal to the crack front and the crack plane (L,M,R in Fig. 1) and the slices were analyzed photoelastically (Ap I) and SIF values were determined for each slice (Ap II). Fringe patterns from the cracked, homogeneous specimen were as expected and are not shown here. Fig. 2 shows the no load (after thermal cycling), after stress freezing (through thickness) and 5th multiple of a side slice for the B-2 specimen and Fig. 3 shows similar results for the B specimen. Clearly, the B specimen shows higher no load residual stresses and, in all cases, a fringe pattern was produced near to the bond line. As will be seen later, the increase in the K_1 due to the bi-material, or modulus effect is believed due to the residual stresses produced by thermal cycling.

TESTS WITHOUT INDUCED RESIDUAL STRESS

Frozen stress tests without the thermal cycling to induce residual stresses were conducted for values of β of 45°, 30°, 15° and 0: Fringe patterns from the homogeneous bonded tests of 0° and 30°, as shown in Fig. 4. For $\beta = 30°$ in the through thickness, no load case, two fringes are visible along the bond line (Fig. 4a). Machining stresses along notch sides tend to anneal out during stress freezing. Upon loading, some twenty fringes appear locally outside the bond line (Fig. 4b). Fig. 4(c) shows the pattern from a slice less than 1mm thick. The dark lines parallel to the bond line denote bond line araldite interfaces.

Fringe patterns for the 0° case are shown in Figs. 4d through 4f. The no load and loaded through thickness patterns are similar to the 30° results qualitatively as is the slice pattern. The no load fringes parallel to the bond line result from bond curing.

In the 15° homogeneous bonded test, a crack emanated from the notch tip under load at the notch tip, ran to a bond-araldite interface and proceeded to grow along the interface.

The normalized SIF results from all tests are tabulated in Table II. Several general comments can be made.

i) All F_{TH} values are two dimensional analytical results. $(F_{II})_{TH}$ values are estimated from $(F_I)_{TH}$ analysis.
ii) The F_I distributions through the thickness revealed a slight elevation in the SIF near mid-thickness as expected in every case except the 45°B-M result.
iii) Only the 15° and the 0° cases revealed a significant increase in $F_1/(F_I)_{TH_{AVG}}$ in the bimaterial specimens (14%, 16%). However, this same order of increase was found for the 0° homogeneous bonded specimen (19%) and would be expected for the 15° case as well.
iv) Values of $(F_{II}/(F_{II})_{TH})_{AVG}$ were generally higher than their $(F_I/(F_I)_{TH})_{AVG}$ counterparts but, since we do not have an accurate two dimensional analytical result for this case, no particular significance is

Table II

F_{TH} = 2D Theoretical estimates

$F_1 = K_1/\bar{\sigma}\sqrt{\pi a}$; $F_2 = K_2/\bar{\sigma}\sqrt{\pi a}$

a = 0.375 in. (9.53 m.m.) [Fig. 1]

B1 = Homogeneous specimen

B2 = Homogeneous bonded specimen

B = Bi-material specimen

LR = Average of left edge and right edge slices [Fig. 1]

LMR = Average of left edge, middle, and right edge slices [Fig. 1]

For $\beta \neq 0$, projections of mode 1 and mode 2 results are used.

Specimen	F_1	F_2	$F_1/(F_1)_{TH}$	$F_2/(F_2)_{TH}$
$\beta = 0^\circ$ (with no-load thermal cycle) ; [Fig. 1] ; $(F_1)_{TH} = 1.51$				
$\bar{\sigma} = 7.00$ psi. (0.048 Mpa.)				
B1-LR	1.70	—	1.13	—
B1-M, LMR	1.64, 1.68	—	1.09, 1.11	—
B2-LR	1.78	—	1.18	—
B2-M, LMR	1.71, 1.75	—	1.13, 1.16	—
B-LR	1.81	—	1.20	—
B-M, LMR	1.91, 1.84	—	1.26, 1.22	—
$\beta = 0^\circ$ (without no-load thermal cycle) ; [Fig. 1] ; $(F_1)_{TH} = 1.51$				
$\bar{\sigma} = 8.75$ psi. (0.060 Mpa.)				
B1-LR	1.37	—	0.907	—
B1-M, LMR	1.67, 1.47	—	1.11, 0.974	—
B2-LR	1.73	—	1.15	—
B2-M, LMR	1.95, 1.80	—	1.29, 1.19	—
B-LR	1.72	—	1.14	—
B-M, LMR	1.82, 1.75	—	1.21, 1.16	—
$\beta = 15^\circ$; [Fig. 1] ; $(F_1)_{TH} = 1.41$; $(F_2)_{TH} = 0.181$				
$\bar{\sigma}_{B1} = 14.0$ psi. (0.097 Mpa.) ; $\bar{\sigma}_{B2} = 8.75$ psi. (0.060 MPa.)				
B1-LR	1.31	0.179	0.929	0.989
B1-M, LMR	1.62, 1.42	0.221, 0.193	1.15, 1.01	1.22, 1.07
B-LR	1.52	0.209	1.08	1.15
B-M, LMR	1.79, 1.61	0.244, 0.231	1.27, 1.14	1.35, 1.28
$\beta = 30^\circ$; [Fig. 1] ; $(F_1)_{TH} = 1.16$; $(F_2)_{TH} = 0.339$				
$\bar{\sigma}_{B1} = 7.00$ psi. (0.048 Mpa.) ; $\bar{\sigma}_{B2,B} = 14.0$ psi. (0.097 MPa.)				
B1-LR	1.03	0.320	0.888	0.944
B1-M, LMR	1.14, 1.07	0.353, 0.330	0.983, 0.922	1.04, 0.973
B2-LR	1.05	0.323	0.905	0.953
B2-M, LMR	1.16, 1.08	0.357, 0.334	1.00, 0.931	1.05, 0.985
B-LR	1.02	0.317	0.879	0.935
B-M, LMR	1.16, 1.07	0.357, 0.330	1.00, 0.922	1.05, 0.973
$\beta = 45^\circ$; [Fig. 1] ; $(F_1)_{TH} = 0.837$; $(F_2)_{TH} = 0.432$				
$\bar{\sigma} = 7.00$ psi. (0.048 Mpa.)				
B1-LR	0.856	0.494	1.02	1.14
B1-M, LMR	0.921, 0.877	0.532, 0.506	1.10, 1.05	1.23, 1.17
B2-LR	0.843	0.486	1.01	1.13
B2-M, LMR	0.873, 0.852	0.504, 0.492	1.04, 1.02	1.17, 1.14
B-LR	0.893	0.516	1.07	1.19
B-M, LMR	0.857, 0.881	0.494, 0.508	1.02, 1.05	1.14, 1.18

attached to these elevations.

v) The residual stress 0° results from the bimaterial specimen were similar to the 0° result for the bimaterial test without thermal cycling suggesting that the mismatch in thermal coefficients between the araldite and the Al-araldite above critical temperature has little effect on the resulting K_1 determination.

SUMMARY

A series of tests were conducted in order to provide a data base for the development of a test for evaluating stress intensity factor distributions along bond lines between incompressible materials of different Moduli of Elasticity. It was desired to separate the bond line effect from the bi-material effect.

In a first test series, residual stress was induced prior to live loads, and fringe patterns from homogeneous, homogeneous bonded, and bimaterial specimens were examined. Table III summarizes the results.

Table III

Specimen	Effect on K_1 (from slicing) of	Percent
B-1	Machining Stresses (MS)	11
B-2	Machining Stress + Bond Line Stress (BS)	16
B	Machining Stress + Bond Line + Modulus	22

As shown in Table II, however, variations in the SIF across the plate thickness were small and of the order of the accuracy of the method of analysis (3.6%). However, they did show the expected distribution in the bimaterial specimen. Moreover, the procedure allows separation of bond stress and bimaterial stress effects.

Tests without induced residual stress were conducted on test specimens containing bond line artificial cracks inclined to the load direction at the angles of 0°, 15°, 30° and 45°. The modulus ratio in the bimaterial specimens was 1.97. Stress intensity factors determined at intervals through the specimens thicknesses by the frozen stress method were normalized with respect to two dimensional solutions for Mode I and two dimensional estimates for Mode II.

As a result of these studies, it was found that:

i) For values of $\beta = 30°, 45°$ (Fig. 1) no increase in the SIF values were observed due either to the bond line or the bimaterial effects.

ii) For values of $\beta = 0°, 15°$ (Fig. 1), an increase in the SIF level occurred, in both cases of 16% and 14% respectively in the bimaterial specimens but results indicate that all of this increase is due to the bondline effect, not the modulus ratio.

iii) Mode II results were larger than predicted by approximate analysis but again appeared due solely to bond line effects.

iv) In all cases except one the peak SIF occurred at mid thickness. In the single exception, ($\beta = 45°$) the variation in the SIF across the thickness appeared to be of the order of the experimental scatter. (*i.e.* $< \pm 3\%$).

v) It is of interest to note that there was no effect on K_1 of either the homogeneous bondline or the bimaterial specimen for values of $\beta = 30°$ and 45°. This is believed due to the fact that the no load bondline fringes were nearly parallel to the load direction near the crack tip and thus made no contribution to the fringe gradient in the load direction which is used to determine K_1.

vi) For both $\beta = 0°$ cases and for $\beta = 15°$, a significant elevation in K_1 occurred in the bimaterial specimens. (14% to 16%). However, this increase also occurred in the homogeneous bonded specimen in the $\beta = 0$ test without residual stress, also to a lesser extent in the $\beta = 0$ homogeneous bonded residual stress test, and is expected in the $\beta = 15°$ homogeneous bonded test. The suggestion is that the elevation of K_1 is due to the bondline stresses and not due to the modulus ratio in the bimaterial specimen. Examination of the no load bondline fringes reveals that they are, indeed nearly normal to the load direction near the crack tip.

In conclusion, it appears that using the three specimen test procedure, reasonable results can be obtained for SIF distributions through the thickness of bimaterial specimens containing bond line cracks in incompressible materials. Tests employing this method are being conducted on cracks parallel to the bond line.

ACKNOWLEDGEMENTS

The authors wish to acknowledge the support of Department of Engineering Science and Mechanics Research Facilities and the support of NASA under Grant No. NAG-1-1622 and Hughes STX Corp. under sub-contract No. 95-7025-K1169.

REFERENCES

[1] Rice, J.R. "Fracture Mechanics Concepts for Interfacial Cracks" *J. Ap. Mech.* V55, pp. 98-103, 1988

[2] Hutchinson, J.W. and Suo, A. "Mixed Mode Cracking in Layered Materials" *Advances in Applied Mechanics* V29 Academic Press, pp. 63-91, 1992.

[3] Smith, C.W., and Kobayashi, A.S. "Experimental Fracture Mechanics" Ch. 20 of *Handbook on Experimental Mechanics*, 2nd Revised Ed. VCH Publishers, pp. 905-968, 1993.

[4] Hasebe, N. and Inohara, S. "Stress Analysis of a Semi-Infinite Plate with an Oblique Edge Crack" *Ing. Arch.* V49, pp. 51-62, 1980

[5] Isida, M. "Tension of A Half Plane Containing Array Cracks, Branched Cracks and Cracks Emanating from Sharp Notches" *Trans. Japan Soc. of Mechanical Engineers* V45 No. 392, pp. 306-317,1979.

[6] Gross, B. Srawley, J.E. and Brown, W. F. Jr. "Stress Intensity Factors for a Single Edge Notched Tension Specimen by Boundary Collocation of a Stress Function" unpublished report NASA Lewis 1964.

[7] Bowie, O.L. "Rectangular Tensile Sheet with Symmetric Edge Cracks" *J. of Ap. Mechanics* V31 Series E. n2 pp. 208-212 June 1964.

[8] Gross, B. and Mendelson A., "Plane Elastoelstic Analysis of V-notched Plates" *Int. J. of Fracture Mechanics*, V8, n3, pp 267-276, 1972.

[9] Post, D., "Fringe Multiplication in Three Dimensional Photoelasticity," *Journal of Strain Analysis*,"Vol. 1, No. 5, pp. 380–388, 1966. la Birefringence des Verres D'optique" *Optics Rev.* V8, pp. 59-69, 1929.

APPENDIX I - FROZEN STRESS PHOTOELASTICITY

When a transparent model is placed in a circularly polarized monochromatic light field, and loaded, dark fringes will appear which are proportional to the applied load. These fringes are called stress fringes or isochromatics and the magnitude of the maximum inplane shear stress is a constant along a given fringe.

Some transparent materials exhibit mechanical diphase characteristics above a certain temperature, called the critical temperature (T_c). The material, while still perfectly elastic will exhibit a fringe sensitivity of about twenty times the value obtained at room temperature and its modulus of elasticity will be reduced to about one six hundredth of its room temperature value. By raising the model temperature above T_c, loading, and then cooling slowly to room temperature, the stress fringes associated with T_c will be retained when the material is returned to room temperature. Since the material is so much more sensitive to fringe generation above T_c than at room temperature, fringe recovery at room temperature fringe upon unloading is negligible. The model may then be sliced without disturbing the "frozen in" fringe pattern and analyzed as a two dimensional model but containing the three dimensional effects. In the use of the method to make measurements near crack tips, due to the need to reduce loads above critical temperature to preclude large local deformations, and the use of thin slices, few stress fringes are available by standard procedures. To overcome this obstacle, a refined polariscope (Fig. I-1) is employed to allow the tandem use of the Post [9] and Tardy [10] methods to increase the number of fringes available locally.

In fringe photographs, integral fringes are dark in a dark field and bright in a bright field. Bright fields are used throughout this paper for clarity.

APPENDIX II (ALGORITHMS)

MODE I ALGORITHM FOR HOMOGENEOUS CASE

Beginning with the Griffith-Irwin Equations, we may write, for Mode I,

$$\sigma_{ij} = \frac{K_1}{(2\pi r)^{\frac{1}{2}}} f_{ij}(\theta) + \sigma^{\circ}_{ij} \qquad (i.j. = n, z) \qquad (II.1)$$

where:

σ_{ij} are components of stress
K_1 is SIF
r, θ are measured from crack tip (Fig. II-1)
σ°_{ij} are non-singular stress components.
Then, along $\theta = \pi/2$, after truncating σ_{ij}

$$(\tau_{nz})_{max} = \frac{K_1}{(8\pi r)^{\frac{1}{2}}} + \tau^\circ = \frac{K_{AP}}{(8\pi r)^{\frac{1}{2}}} \qquad (II.2)$$

where $\tau^\circ = f(\sigma^\circ_{ij})$ and is constant over the data range
K_{AP} = apparent SIF
τ_{nz} = maximum shear stress in nz plane

$$\therefore \frac{K_{AP}}{\bar{\sigma}(\pi a)^{\frac{1}{2}}} = \frac{K_1}{\bar{\sigma}(\pi a)^{\frac{1}{2}}} + \frac{\sqrt{8}\tau^\circ}{\bar{\sigma}} \left(\frac{r}{a}\right)^{\frac{1}{2}} \qquad (II.3)$$

where (Fig. II.1) a = crack length, and $\bar{\sigma}$ = remote normal stress
i.e. $\frac{K_{AP}}{\bar{\sigma}(\pi a)^{\frac{1}{2}}}$ vs. $\sqrt{\frac{r}{a}}$ is linear.
Since from the Stress-Optic Law
$(\tau_{nz})_{max} = \frac{nf}{2t}$ where
n = stress fringe order
f = material fringe value
t = specimen (or slice) thickness
and from Eq. II.2
$K_{Ap} = (\tau_{nz})_{max}(8\pi r)^{\frac{1}{2}} = \frac{nf}{2t}(8\pi r)^{\frac{1}{2}}$,
then K_{Ap} (through a measure of n) and r became the measured quantities from the stress fringe pattern at different points in the pattern.
A typical plot of normalized K_{AP} vs. $\sqrt{r/a}$ for a homogeneous specimen is shown in Fig. II.2.

Mixed Mode Algorithm

The mixed mode algorithm was developed (see Fig. II-3) by requiring that:

$$\lim_{\substack{r_m \to 0 \\ \Theta_m \to \Theta^\circ_m}} \left\{ (8\pi r_m)^{1/2} \frac{\delta(\tau)^{max}_{nz}}{\delta\Theta} (K_1, K_2, r_m, \Theta_m, \tau_{ij}) \right\} = 0 - II - 4$$

which leads to:

$$\left(\frac{K_2}{K_1}\right)^2 - \frac{4}{3}\left(\frac{K_2}{K_1}\right) cot 2\Theta^\circ_m - \frac{1}{3} = 0 - - - II - 5$$

By measuring Θ°_m which is approximately in the direction of the applied load, K_2/K_1 can be determined.
Then writing:

$$\tau^{max}_{nz} = \frac{fn}{2t} = \frac{K^*_{AP}}{(8\pi r)^{\frac{1}{2}}}$$

one may plot $\frac{K^*_{AP}}{\bar{\sigma}(\pi a)^{\frac{1}{2}}}$ vs. $\sqrt{r/a}$ as before, locate a linear zone and extrapolate to $r = o$ to obtain K^*.
Knowing, K^*, K_2/K_1 and Θ°_m, values of K_1 and K_2 may be determined since.

$$K^* = [(K_1 sin\Theta^\circ_m + 2K_2 cos\Theta^0_m)^2 + (K_2 sin\Theta^\circ_m)^2]^{\frac{1}{2}} - - - II - 6$$

Details are found in Ref. 3. A plot of $K^*_{AP}/\bar{\sigma}\sqrt{\pi/a}$ vs. $\sqrt{r/a}$ will yield a linear zone from which K^* can be extracted. Knowing K^* and θ°_m, K_1 & K_2 can be determined from Eqs. II-5 and II-6.

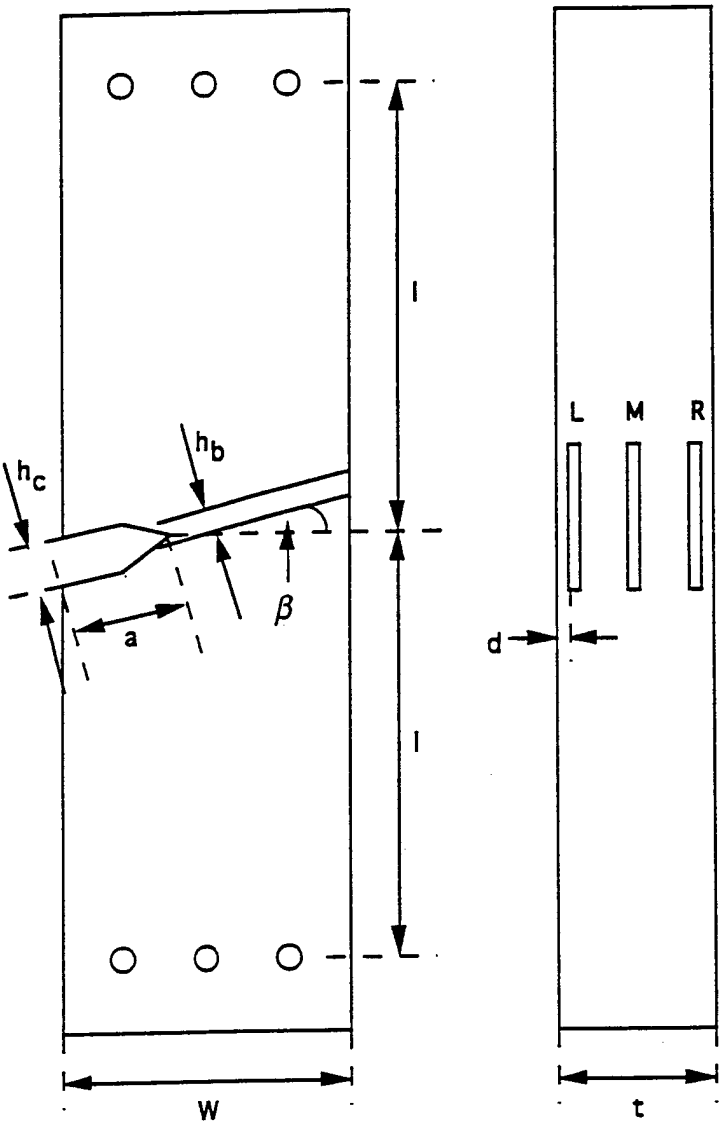

Units	a	W	l	t	h_b	h_c	d
m.m.	9.53	38.1	88.9	12.7	0.356	1.59	1.02
in.	0.375	1.50	3.50	0.500	0.014	0.063	0.040

β = 15, 30 & 45 degrees

Fig. 1 Test Geometry

a) No Load Thru Thickness
After Thermal Cycle

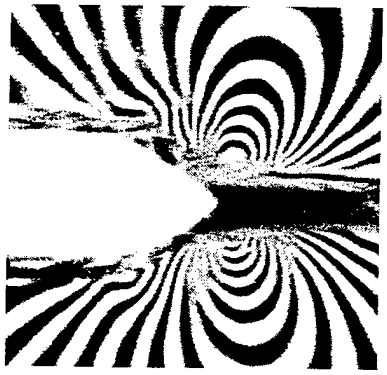

b) After Stress Freezing Thru Thickness

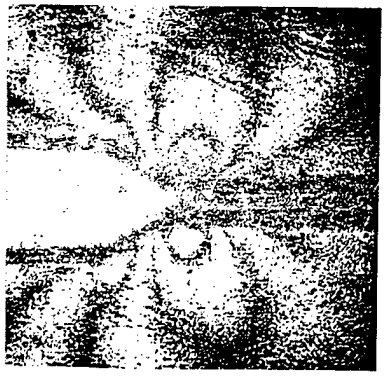

c) 5th Multiple Side Slice

Fig. 2. Homogeneous Bonded Specimen (B-1) with Residual Stress (Bright Field) MF = 8.75

a) No Load Thru Thickness
After Thermal Cycle

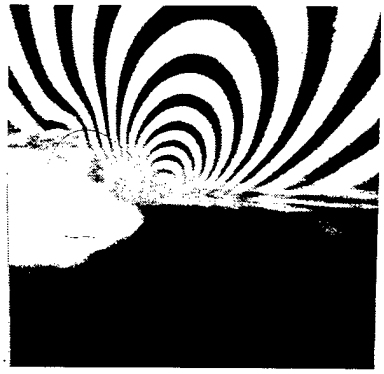

b) After Stress Freezing Thru Thickness

c) 5th Multiple Side Slice

Fig. 3. Bi-Material Specimen (B) With Residual Stress (Bright Field) MF = 8.75

a) No Load Thru Thickness

d) No Load Thru Thickness

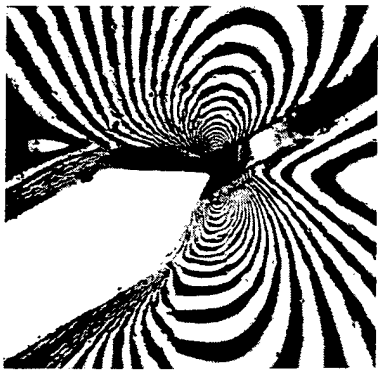

b) Loaded, frozen, thru thickness

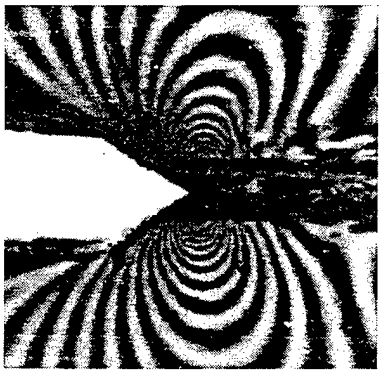

e) Loaded and frozen thru thickness

c) Frozen edge slice

f) Frozen edge slice

Fig. 4 Fringe Patterns - homogeneous bonded specimen bright field Figs. a-c, $\beta = 30°$, Figs. d-f, $\beta = 0°$ M.F. = 8.75 for all figures.

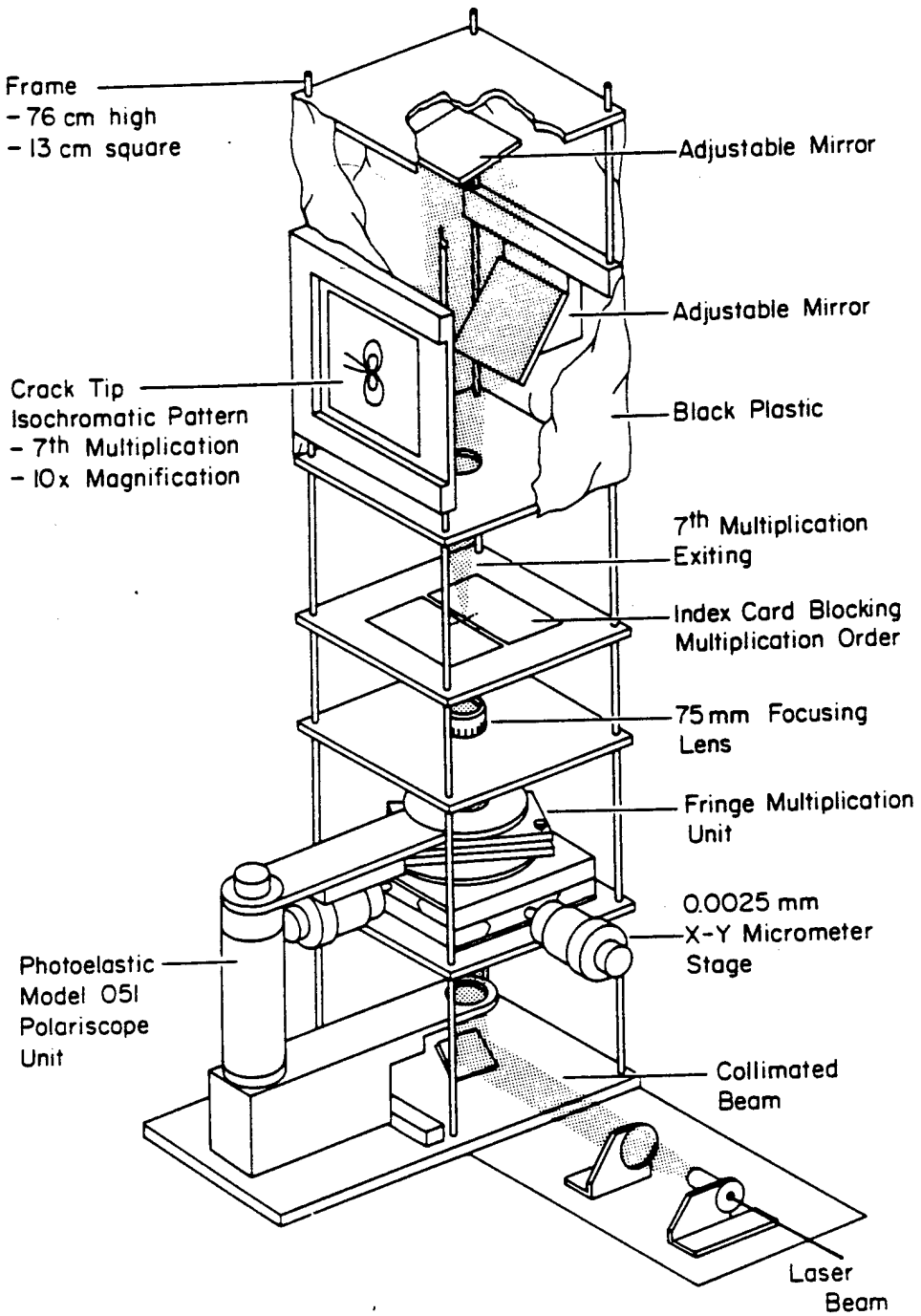

Fig. I-1 Refined Polariscope

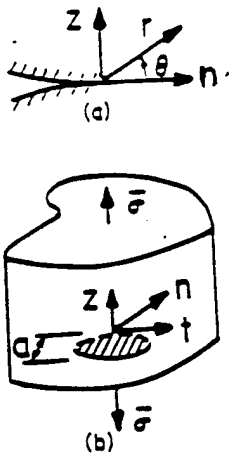

Fig. II-1 Mode 1
Near Tip Notation

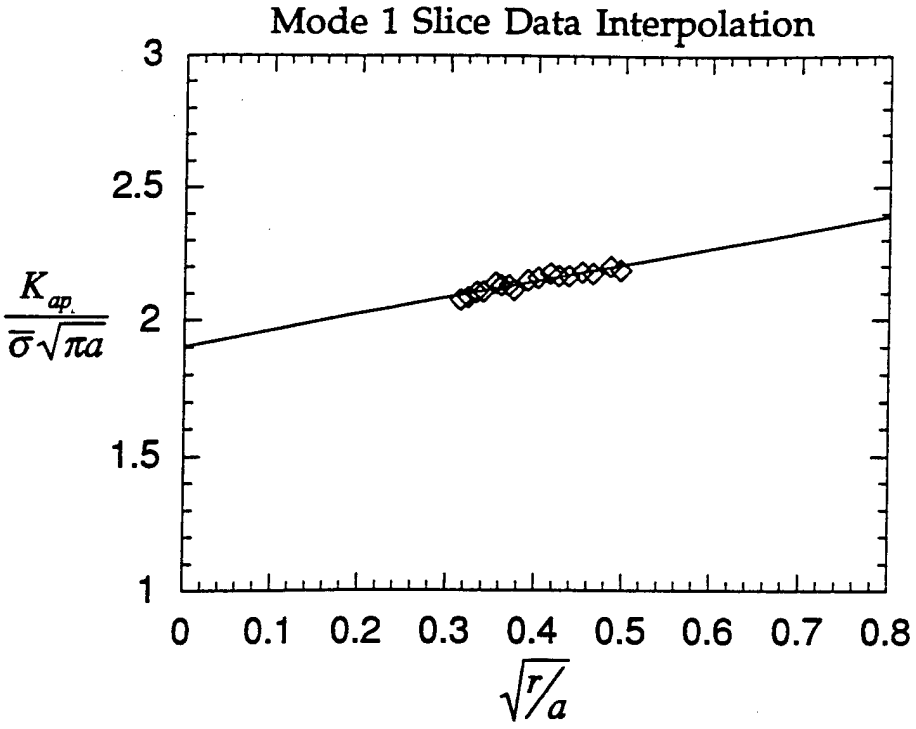

Fig. II-2 Determination of $K_1/\bar{\sigma}\sqrt{r/a}$ from Test Data

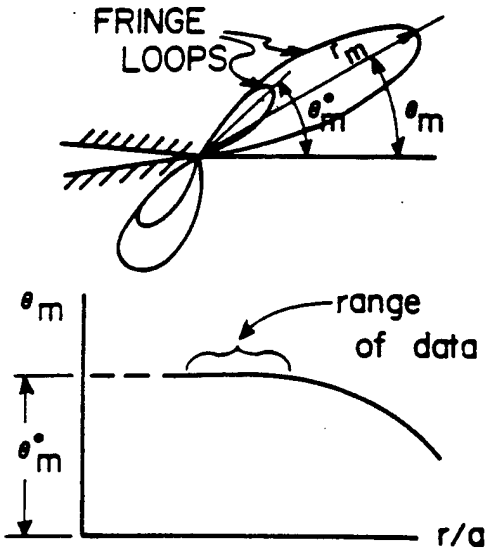

Fig. II-3 Determination of Θ°_m for Mixed Mode Case